Journal of Cluster Science, Vol. 10, No. 2, 1999

Studies on Mesoporous Self-Organizing Aluminosilica

Hong-Ping Lin[1] and Chung-Yuan Mou[2,3]

Received April 17, 1998

A detailed study on the preparation of highly ordered MCM-41 molecular sieves based on our new "delayed neutralization" process is presented. The rate of acidification does not have an apparent effect on the XRD patterns of MCM-41 but affects the morphology. The synthesized products give a thicker constant wall thickness (about 1.70 nm) of mesopore and a sharp pore size distribution. However, the structural order depends on the carbon chain length, the amount of alcohols as cosurfactants, and the synthetic temperature. A tubular morphology of the MCM-41 material, with hollow tubules 0.3 to 3 μm in diameter, can be obtained by careful control of the surfactant–water content and the rate of condensation of silica under high-alkalinity conditions. In tubules-within-a-tubule, the wall of the tubule consists of coaxial cylindrical pores of nanometers characteristic of MCM-41. The hierarchical order structure takes place through a "liquid crystal phase transformation" mechanism in which an anisotropic membrane-to-tubule phase change is involved.

KEY WORDS: M41S; MCM-41; mesoporous molecular sieves; delayed neutralization; hierarchical order; tubules.

INTRODUCTION

The engineering of mesoporosity in materials based on silica is emerging as a new and exciting research area of great scientific and technological importance [1]. The ability to design the porosity, both the size and the wall surface characters, is important in imposing a framework for tailoring catalytic activities and optoelectronic properties of further embedded clusters [2, 3]. The accessible porosity can be utilized as host for conducting or magnetic phases. The composite microstructure is then determined by

[1] Institute of Atomic and Molecular Science, Academia Sinica, P.O. Box 23-166, Taipei, Taiwan.
[2] Department of Chemistry, National Taiwan University, Taipei, Taiwan.
[3] To whom correspondence should be addressed.

1040-7278/99/0600-0271$16.00/0

the pore structure of the host. The electronic and magnetic properties can be tailored by altering the size, shape, and relative concentrations. One could investigate the quantum size effects of clusters in semiconductor, magnetism, and superconductivity [4, 5]. It is a new and exciting field to be explored jointly by chemists, physicists, and engineers.

In the mesoscopic range (1 to 10 nm), many new phenomena can be expected and exploited. The implications are very wide-ranging. One could use the cavity as reaction vessels for reactions involving larger molecules, or in quantum confinement of magnetic or semiconductor materials, or in molecular wires. In recent years, there have been extensive developments in the field of mesoporous aluminosilica materials, where the pores are of manometer size. In particular, the discovery of the new family of mesoporous materials M41S by researchers at Mobil Oil Corp. [6, 7] has attracted great attention from scientists. The pores are created by using surfactant–aluminosilicate self-assembly with surfactant organization as the templates, followed by calcination of the organic part. These mesoporous molecular sieves, with adjustable and uniform pore sizes in the range of 1.5 to 10.0 nm, cover the new range of potential applications. These materials were synthesized with the cationic-type surfactant alkyltrimethylammonium salts $C_nH_{2n+1}(CH_3)_3N^+X^-$ and various silica sources (sodium silicates, TEOS, or silica gel) under hydrothermal conditions. In the solution and gel phases, the system exhibits various complex organizations: cylindrical micelles, hexagonal, cubic, and lamellar phases. And it leads to various final periodic structures of the mesoporous materials, including MCM-41, MCM-48 (cubic), SBA-1, SBA-2, SBA-3, and MSU-X [8, 9]. When one uses an anionic surfactant, some mesostructures of transition element oxides, such as TiO_2, can also be obtained [10]. In addition, Japanese workers invented the mesoporous aluminosilicate FSM-16 with a structure similar to that of MCM-41 by combining Kanemite polysilicate and surfactants [11].

One member of this series, MCM-41, which possesses a hexagonal arrangement of uniformly sized channel mesopores, has been the focus of most recent applications as catalysts, supporters, and advanced materials. This field is exciting not only for the newly available size range of the pores but also in that the self-assembly involves the physics of soft matter, which is very rich in itself [12].

For the purpose of developing catalysis applications, various metals or oxides have been incorporated into MCM-41 materials. Isomorphic substitution of trivalent cations such as Al, B, and Ga into the framework can result in an acid catalyst [13, 14]. For oxidation catalysis, early transition metals such as Ti and V have also been incorporated. Heteropolyacid-supported MCM-41 catalysts can also be made [15, 16]. Using MCM-41

as a support for other more specific catalysts is also a new direction [17]. For example, the large MCM-41 channel can be used to immobilize a metalloporphrin oxidation catalyst. Many of these modified MCM-41 materials show a remarkable increase in catalytic activities [18].

Of these synthesis factors, the silica source seems to be important for the stability of the material at high temperatures. Apparently, silica condensation is the determining process. We have been involved with the study of both the physical chemistry of surfactant self-organization and the synthesis of mesoporous zeolites by inventing a new "delayed neutralization method" [19]. We have made use of developments in these two separate fields.

(i) We used the "delayed neutralization" method in this new process to synthesize MCM-41 materials of a high thermal stability. The effects of variation of the surfactant and experimental factors on the formation of the MCM-41 materials were explored. Factors examined include the chain length, counterion, head group of the surfactant, and addition of a cosurfactant (such as butanol or hexanol). Moreover, the rate of acidification and temperature for synthesis were found to exert an influence on the pore size, the structural order, and the morphology of the MCM-41 material. Furthermore, thermally stable MCM-41 samples could also be obtained at ambient temperature [20].

(ii) We reported that solvent-separated multilayers of periodic hexagonal MCM-41 silicates can be formed at a high alkalinity and further bent into hollow microtubules (micrometer size) with nanochannels forming the walls of these micrometer-sized tubules by careful control of the acidification and the reaction component [21]. The cylindrical silica has the hierarchical order of a tubules-within-tubule structure. The preparation of mesoporous aluminosilicate materials was recently elevated to an exciting new level by the discoveries of hierarchical structures having at least two length scales, micro- and nanometers [22–30]. The ability to control structures on both length scales will have crucial impacts on the catalyst, biomimeralization, and design of nanomaterials. Previously, we reported a tubules-within-a-tubule (TWT) hierarchical order in MCM-41 in hollow tubules 0.3 to 3 μm in diameter. The process is interesting for its self-generating and self-similar hierarchical organization with a high yield ($>95\%$) and uniformity in morphology. In some of the previous works reporting hierarchical order, the micron-scale structure is generated separately, for example, by microemulsion or bacteria

[22, 30], as a template for growing the nanostructure. Our process is, however, through a "liquid crystal phase transformation" mechanism, involving the neat system itself, of anisotropic membrane-to-tubule phase change. A soft intermediate membrane structure of the materials aluminosilicates was responsible for the production of the tubular structure. For the synthesis of MCM-41, when the structure is soft before extensive polymerization of silicates, higher-order organization may thus be controlled and formed. This then opens up whole new approaches to the design of hierarchical orders in inorganic nanomaterials, for many other complex orders can be achieved in complex liquid crystalline phases and modern theories of complex fluids have developed to the extent that they can help us to understand the associated phase changes.

It is the purpose of this paper to report this method.

EXPERIMENTAL

Materials

The silica source was sodium silicate (27% SiO_2, 14% NaOH) from Aldrich. The quaternary ammonium surfactant compounds $C_nH_{2n+1}(CH_3)_3NX$ and $C_nH_{2+1}NC_5H_5X$ (X = Cl, Br, or NO_3) were obtained from Aldrich, Merck, or Tokyo Chemical Industry without further purification. The source of aluminum was sodium aluminate from Riede-de Haën. Sulfuric acid, hydrochloric acid, acetic acid, and nitric acid were obtained from Merck or Janssen Chimica.

Synthetic Procedure

To prepare pure-silica MCM-41 materials, sodium silicate was added to a clear aqueous solution of the surfactant, with stirring, and a gel mixture was formed. After stirring for about 10 min at the synthetic temperature, a proper amount of 1.20 *M* sulfuric acid was added to the gel mixture and the pH value was adjusted to about 8.0–11. Here, two acidification rates were used. One is to add the entire acid to the gel mixture at once—"immediate acidification;" the other is to add the acid drop by drop over about 30 min with a pipette—"gradual acidification." The molar ratio of the resulting gel composition is 1 SiO_2: (1–0.1) surfactant:0.39 Na_2O:0.29 H_2SO_4:(50–400) H_2O. Then, the mixture was stirred for 20 min, loaded into an autoclave, and statically heated at 100°C for

48–144 h. The resulting solid products were recovered by filtration, washed with deionized water, and dried in air at room temperature or 100°C. To remove the organic species occluded in the pores of MCM-41, the as-synthesized samples were calcined in air at 560°C for 6 h.

The aluminosilicate MCM-41 was synthesized by the same process mentioned above except that a suitable amount of sodium aluminate was added to the solution of surfactant in the first step.

Characterization

X-ray powder diffraction (XRD) data were collected on a Scintag X1 diffractometer using CuKα radiation ($\lambda = 0.154$ nm). N_2 adsorption–desorption isotherms were obtained at 77 K on a Micrometric ASAP 2000 apparatus. The sample was outgassed at 300°C for about 6 h at 10^{-3} Torr prior to adsorption. The pore size distribution curves were obtained from analysis of the desorption portion of the isotherms using the BJH (Barrett–Joyner–Halenda) method. Transmission electron micrographs (TEM) were taken on a Hitachi H-7100 operated at 100 keV. Scanning electron microscopy (SEM) was performed on a Hitachi S-2400 or S-800 using an accelerating voltage of 20 keV. Solid-state ^{27}Al MAS NMR experiments were performed at room temperature on a Bruker MSL 500 NMR with a magnetic field of 11 T.

RESULTS AND DISCUSSION

A "Delayed Neutralization" Process for the Synthesis of MCM-41

Acidification Rate

First, we explored the effect of the acidification rate on the MCM-41 products synthesized with different surfactants. Figure 1 shows the products of the C_{16}TMAB–aluminosilicate system at different acidification rates. By gradual control of the rate of acidification, a "tubules-within-a-tubule" (TWT) hierarchical-ordered structure can be obtained (Fig. 1A) [21], which is studied in detailed below. In contrast, the products from immediate acidification have only a microparticle morphology (Fig. 1B). Similar phenomena were observed for MCM-41 products prepared with surfactants of a carbon chain length longer than 12. However, the XRD patterns and pore sizes of all these products are nevertheless independent of the neutralization rate. The delayed neutralization process is a better method for synthesizing highly ordered MCM-41 materials and the hierarchical structure of TWT could be obtained. When a surfactant with a carbon chain

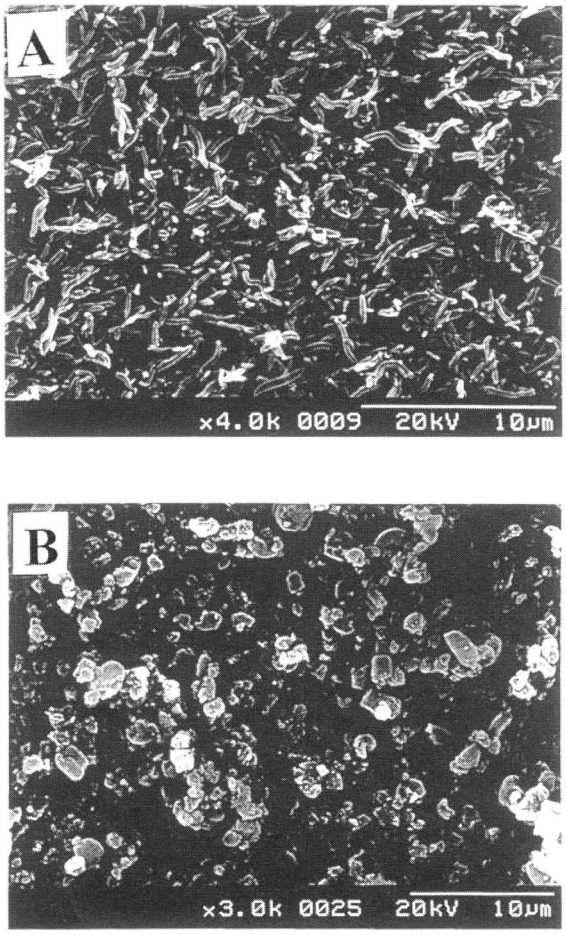

Fig. 1. Scanning electron micrograph (SEM) of the as-synthesized MCM-41 materials prepared from the C_{16}TMAB–alunimosilicate system with Si/Al = 37 using different acidification rates. (A) Gradual acidification; (B) immediate acidification.

length shorter than or equal to 12 was used, the immediate acidification process resulted in products with a more ordered arrangement of hexagonal arrays than those obtained by gradual acidification.

Chain Length

The x-ray diffraction (XRD) patterns of the calcined pure silica MCM-41 products synthesized from alkyltrimethylammonium salts (C_nTMAX; X = B for Br or Cl for Cl, $n = 8$ to 18) with a carbon chain number varying

from 8 to 18 using the immediate acidification process are shown in Figs. 2A–F. It is clearly shown that the d_{100} value increases and the peaks become sharper as the carbon chain length increases. Furthermore, for MCM-41 materials prepared with C_{16}TMAB and C_{18}TMACl surfactants, five XRD peaks appear, indicating that the MCM-41 solids prepared by this new method are as well ordered as the best reported previously [31, 32]. The structure order obtained from most other methods consists of fewer than five XRD peaks [33–36]. The delayed neutralization process leaves more time for the micelles and silica polyanionic species to assemble into a more ordered structure. Nevertheless, the structural order of the MCM-41 products decreased when surfactants of a shorter carbon chain length were used. This is accounted for by the weakening of interactions between the silica polyanionic species and the surfactants with a shorter carbon chain length. In addition, the XRD baselines of all samples are flat at 2θ from 20 to 30°, Implying that few microparticles of amorphous silica are formed using this method. The "delayed neutralization" process offers a convenient procedure to produce highly ordered MCM-41 mesoporous materials with less amorphous silica impurity.

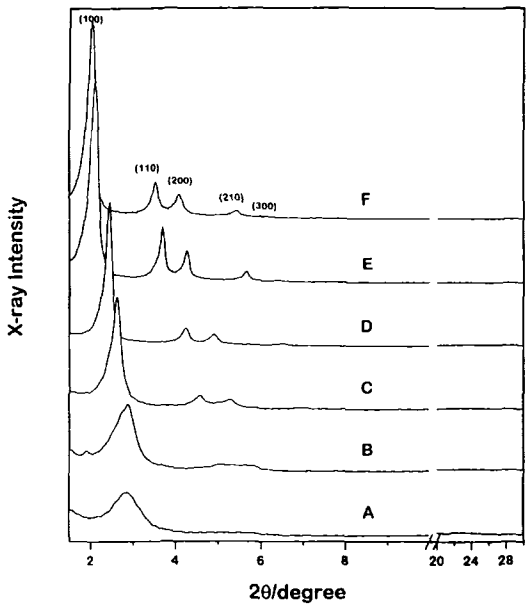

Fig. 2. X-ray powder diffraction patterns of calcined products prepared using the surfactants of different carbon chain length. (A) C_8TMAB; (B) C_{10}TMAB; (C) C_{12}TMAB; (D) C_{14}TMAB; (E) C_{16}TMAB; (F) C_{18}TMACl.

The data on the N_2 adsorption–desorption isotherms of the calcined samples prepared with different surfactants reveal that there is a sharp increase in the adsorbed volume at a certain relative pressure p/p_0, which corresponds to the capillary condensation in the mesopores of the materials. The pore size distributions calculated from N_2 desorption curves are quite narrow (Fig. 3), indicating that this method produces MCM-41 materials of uniformly sized mesopores. Besides, the t-plots of these MCM-41 materials have intercepts close to zero, which indicates that the products have no microporous structures [37, 38].

Table I compares the pore size, d-spacing, and wall thickness of the solids prepared with different carbon chain lengths, counterions, and head groups of the surfactants. The repeat distance (a_0) was calculated by X-ray diffraction data by the equation $a_0 = 2d_{100}/\sqrt{3}$. The wall thickness was determined by the difference between the repeat distance (a_0) and the pore size. These MCM-41 materials have a BET surface area in excess of 1000 m^2/g. The products prepared from surfactants with the same carbon chain length but different counterions and head groups have almost the same pore size and d-spacing, and the pore size and d-spacing increase with

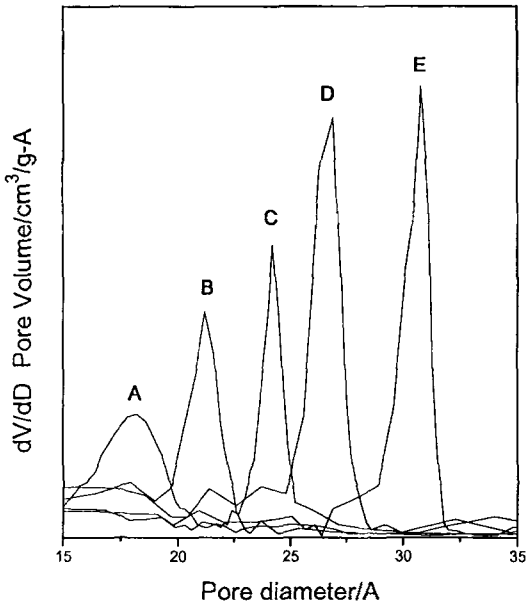

Fig. 3. The pore size distributions of the calcined MCM-41 materials synthesized from different surfactants. (A) C_{10}TMAB; (B) C_{12}TMAB; (C) C_{14}TMAB; (D) C_{16}TMAB; (E) C_{18}TMAB.

Table I. Effect of Surfactant Chain Length, Counterion, Head Group on MCM-41 Pore Size, XRD d_{100} Value, Hexagonal Unit Cell Parameter a_0 and the Wall Thickness (from Ref. 19)

Surfactant	XRD d_{100} (d-spacing/nm)	a_0 (nm)[a]	N_2 pore size (nm)	Wall thickness (nm)
$C_nH_{2n+1}(CH_3)_3NX$[b]				
C_{18}TMAB	4.30	4.96	3.23	1.73
C_{18}TMACl	4.28	4.94	3.18	1.76
C_{16}TMAB	3.96	4.57	2.87	1.70
C_{16}TMACl	3.98	4.59	2.87	1.72
C_{16}TMAN	4.00	4.61	2.86	1.75
C_{14}TMAB	3.61	4.17	2.56	1.61
C_{12}TMAB	3.31	3.82	2.21	1.61
C_{10}TMAB	3.15	3.64	1.92	1.72
C_8TMAB	2.90	3.35	1.67	1.68
$C_nH_{2n+1}NC_5H_5X$[c]				
C_{16}PyB	3.95	4.56	2.72	1.84
C_{16}PyCl	4.01	4.63	2.72	1.91
C_{12}PyCl	3.32	3.83	2.23	1.65

[a] $a_0 = 2d_{100}/\sqrt{3}$ as the distance of nearest pore centers.
[b] Alkyltrimethylammonium halide.
[c] Alkylpyridinium halide.

carbon chain length of the surfactant. This indicates that the counterions bound to the interface of the micelle of the surfactant are replaced by silica polyanionic species during the synthetic process. The head group is relatively small, and the pore size is dependent mainly on the carbon chain length of the surfactant. The wall thickness of all the MCM-41 materials synthesized by this method is in the range of 1.61 to 1.91 nm, quite independent of the surfactants. The more uniform and thicker walls make the MCM-41 materials synthesized by this method more rigid and thermally stable. They shrink less (about 0.12 to 0.22 nm) after calcination and have a sharper pore size distribution (about 0.14–0.23 nm) than those reported previously.

The transmission electron micrographs (TEM) of the calcined samples of C_{16}PyB and C_{12}TMAB illustrate a regular hexagonal array of mesoporous channels (Fig. 4). The repeating distances between pores are in agreement with those obtained from XRD patterns.

Adding Cosurfactant

A surfactant of a shorter carbon chain length has less affinity to combine with the silica polyanionic species, thus the products synthesized from

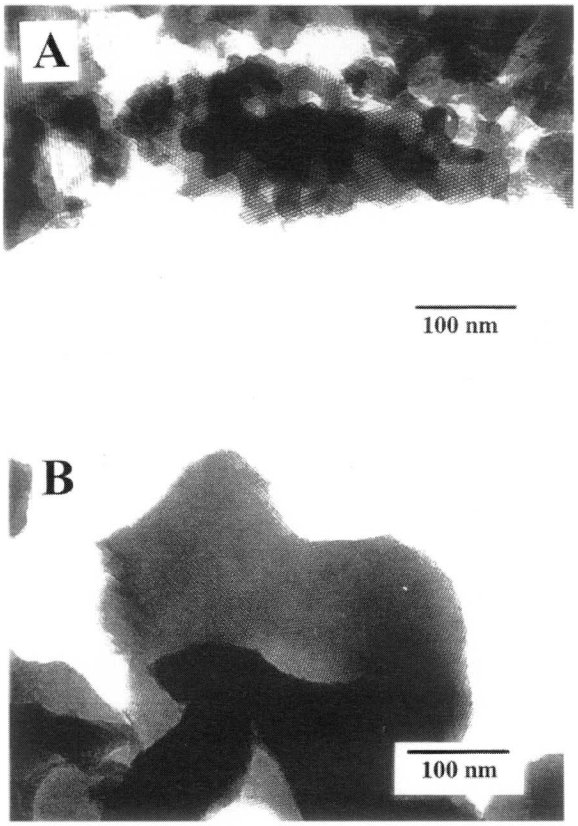

Fig. 4. Transmission electron micrographs (TEM) of the calcined MCM-41 obtained from cationic surfactant-silicate. (A) C_{16}PyB; (B) C_{12}TMAB.

C_8TMAB, C_{10}TMAB, and C_{12}PyCl–silicate systems have less well-resolved XRD patterns and the MCM-41 materials still cannot be synthesized from C_6TMAB. Based on the principle of micelle formation, adding a proper amount of cosurfactant, such as butanol (BuOH) or hexanol (HeOH), could elongate the length of micelles to favor the interaction between micelles and silica polyanionic species [39, 40]. Figure 5 shows that the two diffuse XRD peaks of C_{10}TMAB products can be changed into three or four sharp peaks by adding BuOH or HeOH in a suitable alcohol/surfactant range. But the addition of BuOH or HeOH has no obvious effect on the structure prepared from a surfactant with a shorter carbon chain length (C_6TMAB or C_8TMAB). It is believed that the chain length of C_6TMAB or C_8TMAB is too short to form an energetically favorable

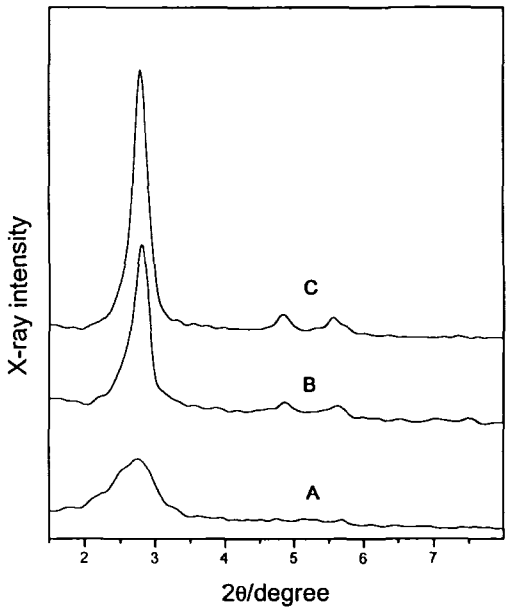

Fig. 5. X-ray powder diffraction patterns of the as-synthesized products prepared from different alcohol/C_{10}TMAB ratios using immediate acidification. (A) BuOH/C_{10}TMAB = 0; (B) BuOH/C_{10}TMAB = 0.65; (C) HeOH/C_{10}TMAB = 0.25.

liquid crystal structure [41]. We concluded that adding short-chain alcohols (BuOH or HeOH) as cosurfactants can improve the formation of the highly ordered hexagonal structure of MCM-41 prepared from shorter-carbon chain surfactants.

Temperature Effect

All of the MCM-41 materials synthesized at room temperature have well-resolved hexagonal XRD patterns, except the product of C_{18}TMAB. Comparing the XRD pattern of the calcined C_{18}TMAB products prepared at room temperature and 50°C (Figs. 6A and C). The latter has four sharp peaks, but the former has just two diffuse peaks. For understanding the effect of temperature on the C_{18}TMAB product, the as-synthesized solids after complete acidification at room temperature and 50°C were also examined. A lamellar mesophase was formed at room temperature, but a hexagonal pattern of MCM-41 was obtained at 50°C (Figs. 6B and D) [42, 43]. The results showed that at room temperature the C_{18}TMAB–silicate system first forms a lamellar mesophase solid, then transforms to an hexagonal final mesoporous MCM-41 product structure during the 100°C

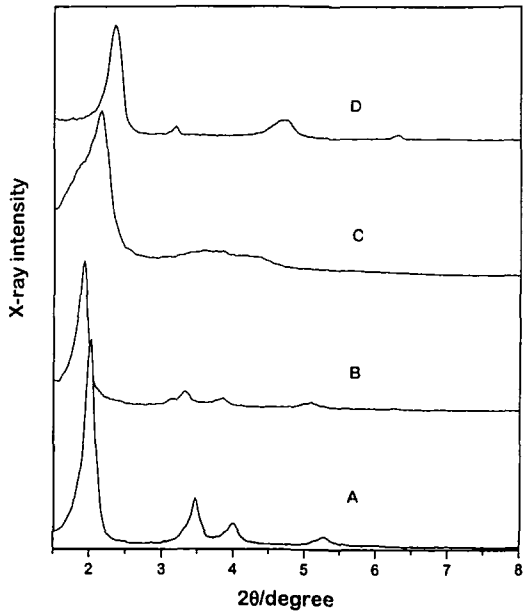

Fig. 6. X-ray powder diffraction patterns of the calcined products of the C_{18}TMAB–silicate system and the as-synthesized solids prepared after complete addition of the acid at different temperate. (A) Calcined product prepared at 50°C; (B) the as-synthesized solid prepared at 50°C; (C) calcined product prepared at room temperature; (D) the as-synthesized solid prepared at room temperature.

hydrothermal reaction. In the high-temperature synthetic case (50°C), a material with a hexagonal structure was formed after neutralization, then the hydrothermal reaction improved it to a more well-ordered structure. This unique character of C_{18}TMAB results from its long carbon chain tending to form a lamellar phase at room temperature. Hence, the formation mechanism and the structure of MCM-41 prepared from surfactants of a longer-carbon chain-length silicate system depend on the synthetic temperature.

Synthesis of MCM-41 at Ambient Temperature

Next we tried the synthesis of MCM-41 at room temperature without hydrothermal reaction [20]. Figure 7 shows the XRD patterns of calcined products synthesized at ambient temperature with an aging time varying from 0 to 30 days. As the aging time increases, the XRD peaks of the calcined material become sharper and more distinct. Four characteristic peaks of MCM-41 were detected in the samples with an aging time equal

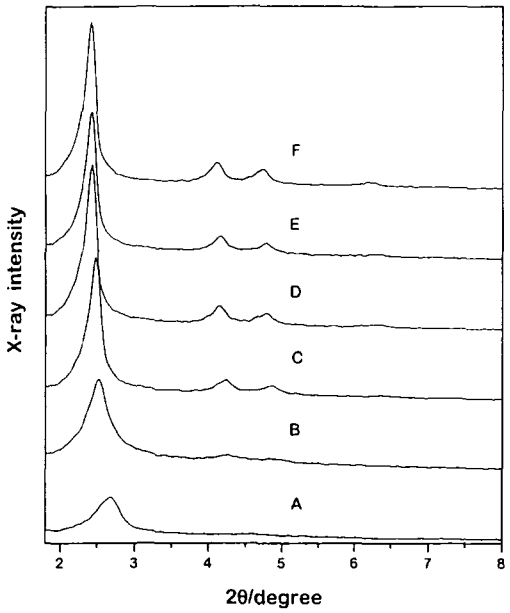

Fig. 7. X-ray powder diffraction patterns of the calcined products of the C_{16}TMAB–silicate system prepared at ambient temperature for different aging times. (A) 0 day; (B) 1 day; (C) 5 days; (D) 10 days; (E) 20 days; (F) 30 days.

or greater than 10 days. It-was found that less aged products have less crystallinity and the d-spacings shrank more after calcination. These results reveal that the condensation of silica walls was almost-complete and the stable MCM-41 structure was formed at ambient temperature after 10 days of aging. It was also found that the characteristic XRD patterns of the samples prepared with different aging times remain intact under prolonged heating at 900°C in air for another 6 h. Compared with the d_{100} of the samples calcined at 550°C, there is only about 0.3 nm of shrinkage. These results indicate that these samples synthesized at ambient temperature have a high thermal stability.

In addition to the synthesis of pure-silica MCM-41 with C_{16}TMAB at ambient temperature, we have also applied the method successfully in the synthesis of pure-silica MCM-41 with different surfactants of hydrocarbon lengths of 10 to 18 carbons (Table II) as well as the synthesis of aluminosilicate MCM-41 with C_{16}TMAB. But we note that room-temperature synthesis generally gives products with a smaller d-spacing (about 0.5- to 0.6-nm differences) and pore diameter compared to those by hydrothermal synthesis (Table I). All samples synthesized by this method have BET surface areas of about 1100 m^2/g.

Table II. The Physical Properties of the MCM-41 Materials Prepared from Different Surfactants at Ambient Temperature and 10-Day Aging (from Ref. 20)

Surfactant	d_{100} (nm)		BET surface area (m^2g^{-1})	Pore diameter (nm)
	As-synthesized	Calcined		
C_{18}TMAB	4.01	3.65	1180	2.63
C_{16}TMAB	3.71	3.38	1064	2.36
C_{14}TMAB	3.50	3.10	1126	2.08
C_{12}TMAB	3.20	2.85	1120	1.86
C_{10}TMAB	2.95	2.62	1132	1.65
C_8TMAB	2.63	2.30	1042	1.32

This new synthesis procedure is also suitable for the formation of aluminosilicste MCM-41. The ^{27}Al MAS NMR spectra of the products with different Si/Al (10–60) ratios show that there is only one peak at about 50 ppm in all as-synthesized samples, indicating that the aluminum atoms are in tetrahedral sites and incorporated in the framework of MCM-41.

Finally, we present some theoretical considerations for explaining the many observations in this section. Although the mesostructures are formed most probably through a cooperative condensation of surfactant and silicate [44, 45], we can divide our theoretical considerations roughly into two parts: the formation of rod-like micelles and the condensation of the hexagonal phase.

We discuss the relation between the micellar structure and the nature of the MCM-41 product obtained. The organization of surfactant depends on the volume (V_H), length (l_c) occupied by the hydrophobic group, and effective surface area (a_0) of the hydrophilic groups of the surfactant. According to packing requirements, the parameter $p = V_H/l_c a_0$ determines the shape of the micelles. When the value of p is in the region of 0 to 1/3, the micelles of the surfactant are spherical; $p = 1/3$ to 1/2 for cylindrical micelles; and $p = 1/2$ to 1 for the lamellar phase. Within the cylindrical micelle range, a higher p value leads to a longer micelle [46, 47].

Let us examine the chain length effect first. Given the same composition in varying surfactant chain length, the effective surface area a_0 is about the same for C_nTMAX. Thus the variation in the p parameter comes from the change in the molecular volume (V_H) and length (l_c). By using the empirical relations [48]

$$V_H(\text{Å}^3) = 27.4 + 26.9n \tag{1}$$

and

$$l_c(\text{A}) = 1.5 + 1.265n \tag{2}$$

one can see that p is an increasing function of n, the number of carbon atoms in the chain. Thus, accordingly, a longer hydrocarbon group in the surfactant would favor a longer micelle, which is empirically true. And a longer rod would lead to more rigid and ordered packing in the hexagonal phase. Therefore, we observed a more well-defined hexagonal structure in MCM-41 as the chain length increases, which is shown in Fig. 2.

The addition of butanol to the surfactant/silicate mixture would lead to longer micelles, as observed in the C_{16}TMAB + salt system in a dynamical light scattering study. This is due to favored entropy of mixing of BuOH or HeOH in longer micelles. Since longer rods stabilize the hexagonal phase, we therefore observe that BuOH or HeOH can improve the hexagonal structure for the case of C_{10}TMAB-made MCM-41.

We have used two counterions, Br^- and Cl^-, in the starting surfactants. As long as the carbon chain length is fixed, they have very little effect on the pore size and lattice d-spacing. This shows that oligosilicates of silicate are the mesostructure-directing agents. Indeed, it has been shown that MCM-41 can be synthesized with a surfactant concentration as low as the critical micelle concentration. After acidification, multidentate oligosilicate (highly charged) would replace both Cl^- and Br^- and form the same hexagonal structure.

The constant wall thickness of roughly 1.7 nm, shown in Table I, is interesting. Previously, researchers have obtained different wall thicknesses, from 0.5 up to 1.7 nm, depending on the alkalinity. The larger pore distance comes with lower alkalinity. Our wall thickness of 1.7 nm seems to be the upper bound. This is because, in the delayed neutralization process, we can reach a pH value as low as 9.5 without the formation of amorphous silica.

As for the effect of temperature, we observed an appreciable effect in the case of C_{18}TMAB. A higher temperature would lead to less counterion association and to a larger a_0 and, thus, a smaller p value. At room temperature, the C_{18}TMAB–silicate system tends to form a lamellar phase, since n is large enough for the hydrophobic effect to dominate. However, at 50°C the p value of C_{18}TMAB will decrease to less than 1/2 and thus it forms a hexagonal phase instead. Further hydrothermal reaction at 100°C would transform the lamellar phase into hexagonal packing since the condensation reaction is carried out at a high temperature, where only the hexagonal phase is stable.

"Tubules-Within-a-Tubule" Hierarchical Order in MCM-41

A tubule-shaped MCM-41 material 0.3 to 3 μm in diameter could be synthesized by careful control of the surfactant–water content and the rate of condensation of silica (gradually acidification) under high-alkalinity conditions. Figure 8A shows a SEM micrograph of the high-yield and uniform tubules of MCM-41 synthesized with C_{16}TMAB. TEM of the sample (Fig. 8B) revealed clear equidistant parallel lines arranged in a regular way along the tubular axis, with an apparent average spacing at $\sim$3.70 nm, which is in reasonable agreement with the XRD result. Therefore, it was supposed that the wall of the tubule consists of coaxial cylindrical channels of nanometers characteristic of MCM-41 and the tubule is hollow. Figure 8C is a schematic description of the "tubules-within-a-tubule" structure order.

To investigate the process of morphological change of this MCM-41 material, we examined the products at different stages of the acidification by XRD pattern and SEM. Before adding H_2SO_4, the surfactant/aluminosilicate mixture appears to be an opaque white suspension. In the early stage of acidification, the mixture undergoes a phase separation to form a surfactant-rich viscous gel phase and a clear aqueous solution. Further addition of acid leads to a sudden dispersion and precipitation of the upper surfactant-rich layer. Figure 9A is an XRD pattern of the as-synthesized material (sample A) at this early stage of neutralization. It is typical for the hexagonal MCM-41. An SEM micrograph of sample A (Fig. 10A) shows, however, a layered lamellar-type structure. Gradual acidification to the mixture leads to another as-synthesized sample, B, in which the XRD pattern maintains the same hexagonal arrangement of MCM-41, with more distinct (110) and (200) peaks (Fig. 9B). The SEM micrograph of sample B shows that the layers in sample A broke up into microtubules (Fig. 10B). After complete addition of acid, the sample completely transforms into tubules with a rather uniform diameter of $\sim$0.3 μm and an average length of $\sim$5 μm. After hydrothermal reaction at 100°C, the filtered sample C gives the XRD pattern in Fig. 9C and the SEM micrograph in Fig. 10C. Calcination of sample C leads to sample D, in which the SEM micrographs show almost the same pattern as in sample C. Examining many of the SEM micrographs, we find that the tubular form represents $>$95% of the solid material.

The calcined product was further characterized by N_2 adsorption–desorption isotherm. It gives a BET surface area of about 1000 m^2/g. The pore size distribution shows an average pore size of about 2.6 nm and a half-height width of 0.2 nm. The ^{27}Al nuclear magnetic resonance spectroscopy of the as-synthesized material shows a peak only at 52 ppm, indicating that all of the aluminum resides in the skeleton.

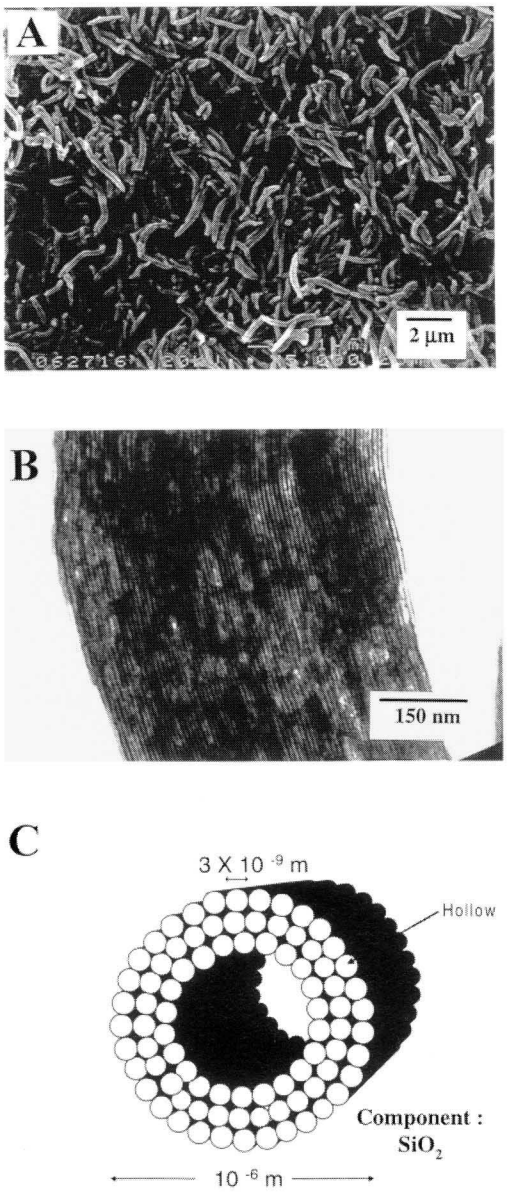

Fig. 8. The MCM-41 material obtained from a gel mixture with a mole ratio, 1 Al_2O_3:75 SiO_2:30 Na_2O:35 C_{16}TMAB:6500 H_2O. (A). Scanning electron microscopy (SEM) of the microsized tubular product. (B) Transmission electron micrograph of the tubular aluminosilicate MCM-41 material. (C) The schematic diagram of the "tubules-within-a-tubule" hierarchical structure.

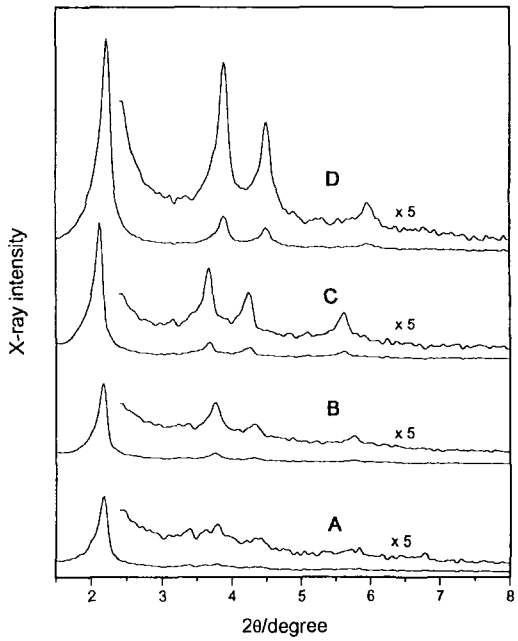

Fig. 9. Powder x-ray diffraction patterns of mesostructure precipitated from a same mixture with a mole ratio, 1 Al_2O_3:75 SiO_2:30 Na_2O:35 C_{16}TMAB:6244 H_2O at various synthetic stages. (A) Sample A: $H_2SO_4/Al_2O_3 = 5.7$. (B) Sample B: $H_2SO_4/Al_2O_3 = 17.0$. (C) Sample C: After complete addition of acid ($H_2SO_4/Al_2O_3 = 21.6$) and hydrothermal reaction. (D) Sample D: After calcination of Sample C.

The higher-order hierarchical silica structures we found here have been extensively documented in the ultrastructure of the siliceous skeletons of marine diatoms and radiolarian. The hollow tubular valve, with the large central area absent, of the diatom species *Annellus californicus* [49], in fact looks strikingly similar to the hollow tubular structure we report here. The diatoms and radiolaria are usually on the micrometer length scale. In contrast, synthetic chemistry normally achieve a self-organization pattern only in the nanometer range. In this report, we have demonstrated that such higher-order biomimetic self-organization can be accomplished in laboratory chemistry.

There are two experimental factors that are crucial in the formation of hollow microtubules: the ratio of surfactant to water in the reactant and the delayed slow neutralization procedure. Although there is a large range of surfactant/water ratios conducive to the formation of periodical hexagonal-phase MCM-41, the corresponding range ratio for forming hollow microtubules is relatively narrow. If the C_{16}TMAB/water ratio is too low,

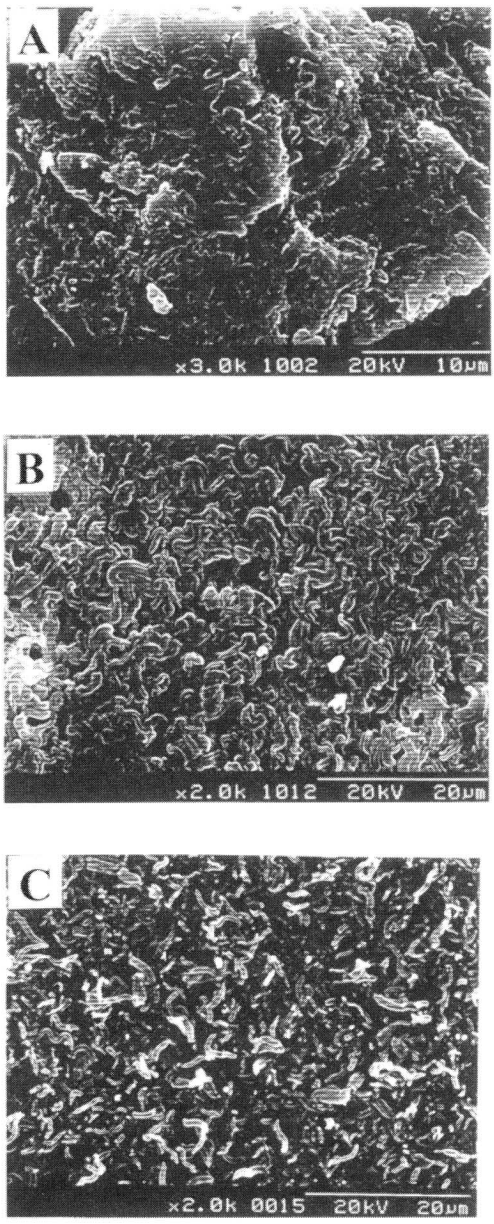

Fig. 10. Scanning electron micrographs of the morphology formed at various stages of synthesis of aluminosilicate MCM-41 with the same materials as in Fig. 9. (A) Sample A; (B) Sample B; (C) Sample C.

the morphology of the product is the usual micro-particle morphology. The neutralization step should also be slow. It seems that, in this way, the hollow tubule structure can thus be formed under high pH conditions before substantial polymerization of silicates lead to rigid, unbending structures.

The almost-complete transformation of the aluminosilicate under mild reaction conditions into a uniform size of hollow tubules leads us to propose a "liquid crystal phase transformation" mechanism for the formation of the new structure. In the beginning, under high pH conditions, the silicate/surfactant system was close to the lamellar/hexagonal phase boundary. A small extent of acidification results in a mixed lamellar/hexagonal phase in which layers of hexagonally arranged rod micelles are separated by bilayers of surfactants and water as shown in Fig. 11A. It probably corresponds to the intermediate phase reported in the surfactant phase diagram. The layered structure could be stabilized by the electrostatic and entropic undulation repulsion force between the membrane layers [50].

Since the membrane layers are intrinsically anisotropic, further acidification leading to condensation of silicates and charge imbalance on the membrane surface would favor curvature of the membrane along only one direction (Fig. 11B), the trans-rod direction. Further, neutralization would then bend the membrane completely into tubules as shown in Fig. 11C. A "natural wavelength" of destabilization can thus be expected and leads to uniform diameters of tubules as we observed. The transformation of lamellar → ripple → tubular phase is in parallel with the known process in the formation of lipid tubules [51–53]. Multilamellar lipid tubules have been observed through a first-order phase transition recently. Theoretically,

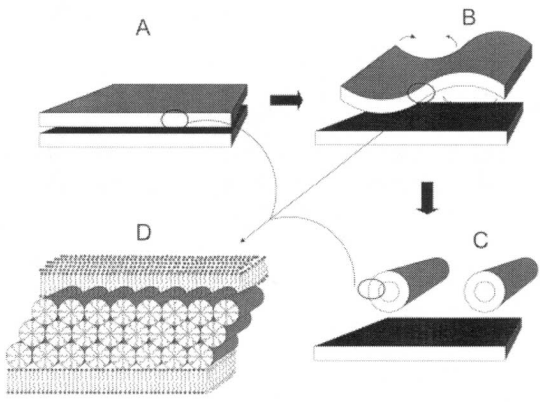

Fig. 11. Proposed mechanism for the formation of microtubular morphology of MCM-41.

it has been predicted that fluctuating tethered membranes with any intrinsic anisotropy unavoidably transform themselves into "new" tubules, given enough driving force. In our case the driving force arises from the charge imbalance at the surface associated with the condensation reaction of the silicate–oxygen bond as the pH is lowered. The "liquid crystal phase transformation" mechanism proposed in this report could provide a new paradigm toward understanding higher-order biominerization.

CONCLUSION

The delayed neutralization process is a preferred method to synthesize highly ordered MCM-41 with thicker walls and sharper pore size distributions. It also provides us a way to explore the interaction between the micelles of the surfactants with different carbon chain lengths, counterions, or head groups and the silica ployanionic species. During this procedure, we could progressively probe the intermediates of the surfactant–silicate system in order to understand completely the formation mechanism of MCM-41 and to control the synthetic condition in order to obtain desirable MCM-41 materials.

In addition, a strategy of producing a hollow tubular form of MCM-41 that is based on the sequential separation of self-organization of template/silicate and polymerization of silicates is presented. One can build the more complex tubules-within-tubule structure through a phase transformation of liquid crystal by delaying the formation of the rigid structure. This may give us a new way to explore the many rich complex structures that are possible in surfactant systems and to form some new zeolite structures. The ability to control synthetically the intricate hollow tubular form of the aluminosilicate MCM-41 could find important applications in catalysis, separation technology, and opticoelectronics.

ACKNOWLEDGMENTS

We thank Prof. Soofin Cheng, Shang-Bin Liu, and Ms. Yah-Ru Cheng for many helpful discussions. This research was supported by the Nation Science Council of Taiwan (NSC 85-2113-31-M-002-032 cc).

REFERENCES

1. H. Schaefer (1994). *MRS Bull.* **19**, 14.
2. G. A. Ozin and C. Gil (1989). *Chem. Rev.* **89**, 1749.
3. S. L. Gillet (1996). *Nanotechnology* **7**, 168.
4. G. D. Stucky and J. E. MacDaugall (1990). *Science* **247**, 669.

5. D. D. Awschalom, D. P. DiVincenzo, and J. F. Smyth (1992). *Science* **258**, 414.
6. C. T. Kresge, M. E. Leonowicz, W. J. Roth, J. C. Vartuli, and J. S. Beck (1992). *Nature* **359**, 710.
7. J. S. Beck, J. C. Vartuli, W. J. Roth, M. E. Leonowicz, C. T. Kresge, K. D. Schmitt, C. T.-W. Chu, D. H. Olson, E. W. Sheppard, S. B. Higgins, and J. L. Schlenker (1992). *J. Am. Chem. Soc.* **114**, 10834.
8. G. D. Stucky (1996). 11th International Zeolite Conference, Plenary Lecture, Seoul Korea.
9. (a) S. A. Bagshaw, E. Prouzet, and T. J. Pinnavaia (1995). *Science* **269**, 1242; (b) S. A. Bagshaw, F. Direnzo, and F. Fajula (1996) *Chem. Commun.* 2209.
10. D. M. Antonelli and J. Y. Ying (1995). *Angew. Chem. Int. Ed. Engl.* **34**, 2014.
11. (a) S. Inagaki, Y. Fukushima, and K. Kuroda (1993). *J. Chem. Soc. Chem. Commun.* 680; (b) T. Yanagisawa, T. Shimizu, K. Kuroda, and C. Kato (1990). *Bull. Chem. Soc. Japan* **63**, 988.
12. W. M. Gelbart and A. Ben-Shaul (1996). *J. Phys. Chem.* **100**, 13169.
13. Z. Luan, H. He, W. Zhou, C.-F. Cheng, and J. Klinowski (1995). *J. Chem. Soc. Faraday Trans.* **91**, 2955.
14. C.-F. Cheng, Z. Luan, and J. Klinowski (1995). *Langmuir* **11**, 2815.
15. P. T. Tanev, M. Chibwe, and T. J. Pinnavaia (1994). *Nature* **368**, 321.
16. K. M. Reddy, I. Moudrakovski, and A. Sayari (1994). *J. Chem. Soc. Chem. Commun.* 1059.
17. A. Sayari (1996). *Chem. Mater.* **8**, 1840.
18. By now there is already a large patent literature providing a wealth of information about the use of MCM-41 as a catalyst for petrochemical applications. For a short review in the published literature, see Ref. (17).
19. H. P. Lin, S. Cheng, and C.-Y. Mou (1996). *Microporous Mater.* **10**, 111.
20. H. P. Lin, S. Cheng, and C.-Y. Mou (1996). *J. Chin. Chem. Soc.* **43**, 375.
21. H. P. Lin, S. Cheng, and C.-Y. Mou (1996). *Science* **273**, 765.
22. S. Schacht, Q. Hou, I. G. Voigtmartin, G. D. Stucky, and F. Schüth (1996). *Science* **273**, 768.
23. (a) S. Mann and G. A. Ozin (1996). *Nature* **382**, 313; (b) H. Yang, N. Coombs, I. Sokolov, and G. A. Ozin (1996). *Nature* **381**, 589.
24. (a) P. T. Tanev and T. J. Pinnavaia (1996). *Science* **271**, 1267; (b) P. T. Tanev, Y. Liang, and T. J. Pinnavaia (1997). *J. Am. Chem. Soc.* **119**, 8616.
25. M. Grün, I. Lauer, and K. K. Unger (1997). *Adv. Mater.* **9**, 254.
26. H. Hou, Q. J. Feng, F. Schüth, and G. D. Stucky (1997). *Chem. Mater.* **9**, 14.
27. (a) H. Yang, N. Coombs, and G. A. Ozin, (1997). *Nature* **386**, 692; (b) A. Ozin, G. H. Yang, I. Sokolov, and N. Coombs (1997). *Adv. Mater.* **9**, 662.
28. S. Mann and G. A. Ozin (1996). *Nature* **382**, 313.
29. (a) I. A. Aksay, M. Trau, S. Mann, I. Honma, N. Yao, L. Zhou, P. Fenter, P. M. Eisenberger, and S. M. Gruner (1996). *Science* **273**, 892; (b) K. M. McGrath, D. M. Dabbs, N. Yao, I. A. Aksay, and S. M. Gruner (1997). *Science* **277**, 552.
30. S. A. Davisd, S. L. Burkett, N. H. Mendelson, and S. Mann (1997). *Nature* **385**, 420.
31. (a) J. M. Kim, J. H. Kwak, S. Jun, and R. Ryoo (1995). *J. Phys. Chem.* **99**, 16742; (b) R. Ryoo and S. Jun (1997). *J. Phys. Chem. B* **101**, 317.
32. (a) J. W. White (1997). *Langmuir* **13**, 6363; (b) K. J. Edler and J. W. White (1997). *Chem. Mater.* **9**, 1226.
33. A. Monnier, F. Schüth, Q. Huo, D. Kumar, D. Margolese, R. S. Maxwell, G. D. Stucky, M. Krishnamurty, P. Petroff, A. Firouzi, M. Janicke, and B. F. Chmelka (1993). *Science* **261**, 1299.

34. N. Coustel, F. D. Renzo, and F. Fajula (1994). *J. Chem. Soc. Chem. Commun.* 967.
35. A. Sayari, I. Moudrakovski, C. Danumah, C. I. Ratcliffe, J. A. Ripmeester, and K. F. Preston (1995). *J. Phys. Chem.* **99**, 16373.
36. (a) C. F. Cheng, Z. Luan, and J. Klinowski (1995). *Langmuir* **11**, 2815; (b) J. S. Beck, J. C. Vartuli, G. J. Kennedy, C. T. Kresge, W. J. Roth, and S. E. Schramm (1994). *Chem. Mater.* **6**, 1816.
37. P. J. Branton, P. G. Hall, and K. S. W. Sing (1993). *J. Chem. Soc. Chem. Commun.* 1257.
38. P. J. Branton, P. G. Hall, K. S. W. Sing, H. Reichert, F. Schüth, and K. K. Unger (1994). *J. Chem. Soc. Faraday Trans.* **90**, 2965.
39. S. Candau and R. Zaana (1981). *J. Colloid Interface Sci.* **84**, 206.
40. M. Almgren and S. Swarup (1983). *J. Colloid Interface Sci.* **91**, 256.
41. G. J. Tiddy (1980). *Phys. Rev.* **57**, 1.
42. C. Y. Chen, S. Q. Xiao, and M. E. Davis (1995). *Microporous Mater.* **4**, 1.
43. (a) C. Y. Chen, H. X. Li, and M. E. Davis (1993). *Microporous Mater.* **2**, 17; (b) C. Y. Chen, S. L. Burkett, H. X. Lin, and M. E. Davis (1993). *Microporous Mater.* **2**, 27.
44. (a) Q. Huo, D. I. Margolese, U. Ciesla, D. G. Demuth, P. Feng, T. E. Gier, P. Sieger, A. Firouzi, B. F. Chmelka, F. Schüth, and G. D. Stucky (1994). *Chem. Mater.* **6**, 1176; (b) Q. Hou, R. Leon, P. M. Petroff, and G. D. Stucky (1995). *Science* **268**, 1324; (c) Q. Hou, D. I. Margolese, and G. D. Stucky (1996). *Chem. Mater.* **8**, 1147.
45. A. Firouzi, D. Kumar, T. Besier, P. Sieger, Q. Huo, S. A. Walker, J. A. Zasadzinski, C. Glinka, J. Nicoi, D. Margolese, G. D. Stucky and B. F. Chmelka (1995). *Science* **267**, 1138.
46. J. N. Israolachvili, D. J. Mitchell, and B. W. Ninham (1976). *J. Chem. Soc. Faraday Trans.* 2 **72**, 1525.
47. D. Langevin (1992). *Annu. Rev. Phys. Chem.* **43**, 341.
48. C. Tanford, *The Hydrophobic Effect* (Wiley, New York, 1973).
49. W. Helfrich (1978). *Z. Naturforsch.* **33a**, 305.
50. L. H. Burckle, *in* B. U. Haq and A. Boersna (eds.), *Introduction to Marine Micropaleontology* (Elsevier, Amsterdam, 1979), pp. 245–275.
51. J. M. Schnur (1993). *Science* **262**, 1669.
52. B. N. Thomas, C. R. Safinya, R. J. Plano, and N. A. Clark (1995). *Science* **267**, 1635.
53. L. Radzihovsky and J. Toner (1995). *Phys. Rev. Lett.* **75**, 4752.